

*Electronic Supplementary Information*

Tuning intramolecular electron transfer of cyanide bridged [Co<sub>2</sub>Fe<sub>2</sub>]  
squares through chemical modifications in solid and solution

Pei-Ye You <sup>a</sup>, Rong-Jia Wei,<sup>\*a</sup> Mo Xie,<sup>a</sup> Guo-Hong Ning,<sup>a</sup> and Hiroki Oshio<sup>\*b,c</sup>

<sup>a</sup>College of Chemistry and Materials Science, Guangdong Provincial Key Laboratory of Functional Supramolecular Coordination Materials and Applications, Jinan University, Guangzhou, Guangdong 510632, P. R. China

<sup>b</sup>Faculty of Pure and Applied Sciences, Department of Chemistry, University of Tsukuba, Tennodai 1-1-1, Tsukuba 305-8571, Japan.

<sup>c</sup>State Key Laboratory of Fine Chemicals, Dalian University of Technology, Dalian 116024, China

\*Corresponding authors: [rjwei@jnu.edu.cn](mailto:rjwei@jnu.edu.cn);

[oshio@chem.tsukuba.ac.jp](mailto:oshio@chem.tsukuba.ac.jp).

## **Contents**

- 1. Experimental section**
- 2. Photos for solid samples of the complexes**
- 3. X-ray crystallographic studies**
- 4. Powder X-ray diffraction (PXRD)**
- 5. Magnetic measurements**
- 6. Thermogravimetric analyses (TGA)**
- 7. Fourier-transform infrared (FT-IR) spectra**
- 8.  $^{57}\text{Fe}$  Mössbauer spectra**
- 9. Various temperature UV-vis-NIR spectra in solution state**
- 10. Electrochemical studies**
- 11. Theoretical calculation**
- 12. References**

## 1. Experimental section

### Materials and Method

TBA[Fe<sup>III</sup>(Tp')(CN)<sub>3</sub>] (TBA = tetra-*n*-butylamine) was prepared according to the literature<sup>1</sup>. All other chemicals and reagents were commercially available and used without further purification. were purchased from commercial sources and used without further purification. Magnetic susceptibility data were collected using a Quantum Design MPMS-5S SQUID magnetometer with an applied magnetic field of 5 kOe and temperature scan rate of 1 K/min. Pascal's constants were used to determine the diamagnetic corrections. Infrared absorption spectra were measured on KBr pellet samples using a SHIMADZU IR Affinity-1 spectrometer. UV-vis-NIR absorption spectra were recorded on SHIMADZU UV-3150 spectrometer. The temperature dependence of UV-vis-NIR absorption spectra was measured using a SHIMADZU UV-3150 spectrometer equipped with UNISOKU USP-203-A cryostat. <sup>57</sup>Fe Mössbauer spectra were collected on a WSS-10 spectrometer equipped with a Jains Cryostat. The spectrometer was calibrated using standard  $\alpha$ -Fe foil at room temperature. Elemental analyses for C, H, and N were performed on Perkin-Elmer 240Q elemental analyzer. Powder X-ray diffraction (PXRD) data was collected at 40 kV, 30 mA using microcrystalline samples on a Rigaku Ultima IV diffractometer using Cu-K $\alpha$  radiation ( $\lambda = 1.5418 \text{ \AA}$ ). The measurement parameters include a scan speed of 0.5 °/min, a step size of 0.02°. Cyclic voltammetry for the complexes were measured in a standard one-compartment cell under nitrogen at room temperature by a BAS 620A electrochemical analyzer with a platinum-wire counter electrode, an SCE reference electrode, and a glassy carbon (GC) working electrode. The experiments were carried out in MeCN with 0.1 M TBAPF<sub>6</sub> as supporting electrolyte.

### Synthesis of {[Co(bpy)<sub>2</sub>]<sub>2</sub>[Fe(tp')(CN)<sub>3</sub>]<sub>2</sub>}(PF<sub>6</sub>)<sub>2</sub> (1)

Co(BF<sub>4</sub>)<sub>2</sub>·6H<sub>2</sub>O (17 mg, 0.05 mmol) and bpy (23.4 mg, 0.15 mmol) were dissolved in 10 mL ethanol to give an orange solution, which was combined with a 10 mL methanol solution containing TBA[Fe<sup>III</sup>(Tp')(CN)<sub>3</sub>] (31.5 mg, 0.05 mmol) and TBAPF<sub>6</sub>

(19.4 mg, 0.05 mmol). The resulting red solution was allowed to stand overnight to give **1** as red block crystals. Yield: 19.1 mg (42.1%). Elemental analysis (%) calcd for  $C_{70}H_{64}B_2Co_2F_{12}Fe_2N_{26}P_2$ : C, 46.44, H, 3.56, N, 20.11; found: C 46.20, H 3.50, N 19.77.

#### **Synthesis of $\{[Co(dmbpy)_2][Fe(tp')(CN)_3]\}_2(PF_6)(OTf) \cdot 2MeOH$ (**2**)**

$Co(OTf)_2 \cdot 6H_2O$  (23 mg, 0.05 mmol) and dmbpy (27.6 mg, 0.15 mmol) were dissolved in 5 mL ethanol to give an orange solution, which was combined with a 5 mL methanol solution containing  $TBA[Fe^{III}(Tp')(CN)_3]$  (31.5 mg, 0.05 mmol) and  $TBAPF_6$  (19.4 mg, 0.05 mmol). The resulting red solution was allowed to stand overnight to give **2** as dark red block crystals. Yield: 17.4 mg (35.2%). Elemental analysis (%) calcd for  $C_{79}H_{80}B_2Co_2F_9Fe_2N_{26}O_3PS \cdot H_2O$ : C, 48.79, H, 4.25, N, 18.72; found: C 48.55, H 4.16, N 18.68.

#### **Synthesis of $\{[Co(dtbbpy)_2][Fe(tp')(CN)_3]\}_2(PF_6)(OTf) \cdot 2MeOH \cdot 3EtOH$ (**3**)**

$Co(OTf)_2 \cdot 6H_2O$  (23 mg, 0.05 mmol) and dtbbpy (40 mg, 0.15 mmol) were dissolved in 2 mL ethanol to give an orange solution, which was combined with a 2 mL methanol solution containing  $TBA[Fe^{III}(Tp')(CN)_3]$  (31.5 mg, 0.05 mmol) and  $TBAPF_6$  (19.4 mg, 0.05 mmol). The resulting red solution was allowed to stand overnight to give **3** as green block crystals. Yield: 153. Mg (24.1%). Elemental analysis (%) calcd for  $C_{107}H_{140}B_2Co_2F_9Fe_2N_{26}O_5PS \cdot 3H_2O$ : C, 53.33, H, 6.11, N, 15.11; found: C 53.09; H 5.78; N 15.52.

## 2. Photos for solid samples of the complexes



**Fig. S1** Photo of complex 1.



**Fig. S2** Photo of complex 2.

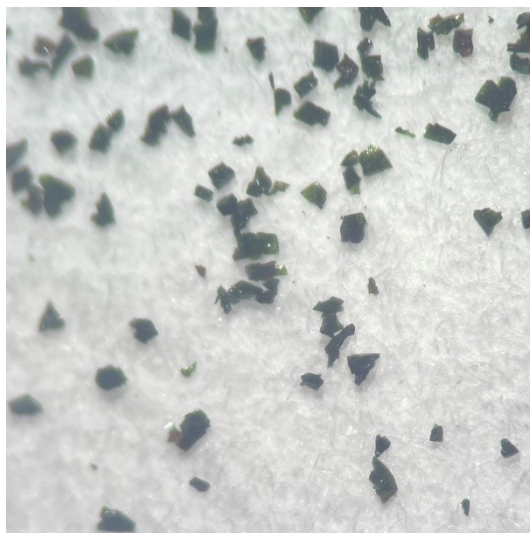


**Fig. S3** Photo of complex 3.

### 3. Powder X-ray diffraction (PXRD).

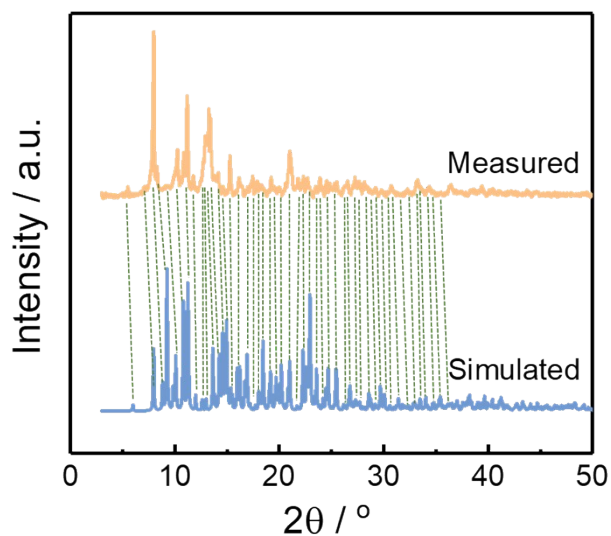


**Fig. S4** PXRD of 1. The crystals shown in Fig. S1 was used for the PXRD measurement. The experimental PXRD pattern is comparable to the simulated counterpart, but with different intensities for the reflections, due to the strong preferential orientation for the crystal sample. Fine grind resulted in the loss of crystallinity.

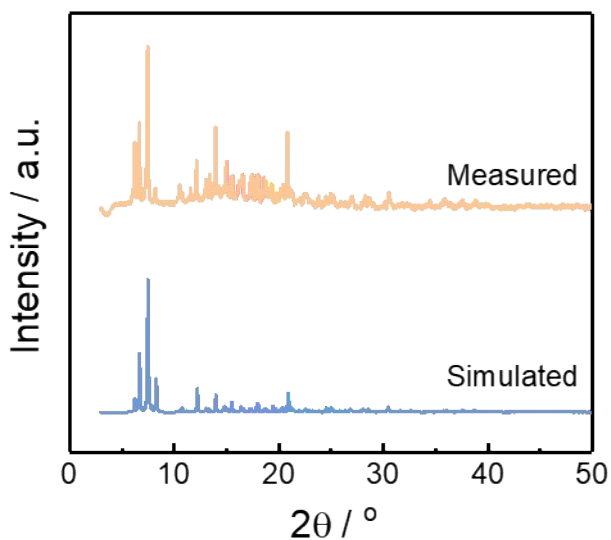


**Fig. S5** PXRD of 2.

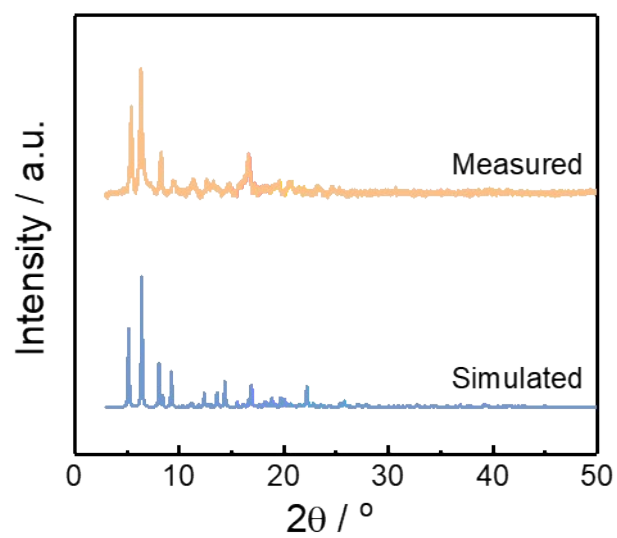


**Fig. S6** PXRD of **3**.

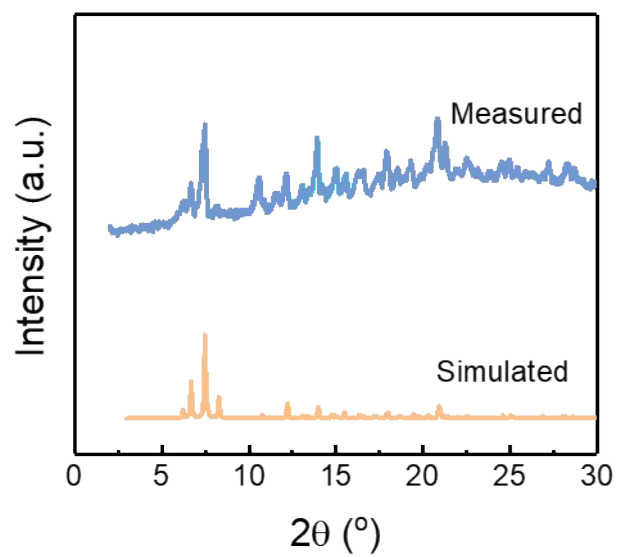


**Fig. S7** PXRD of **2** after magnetic measurement upon temperature increased to 320 K.

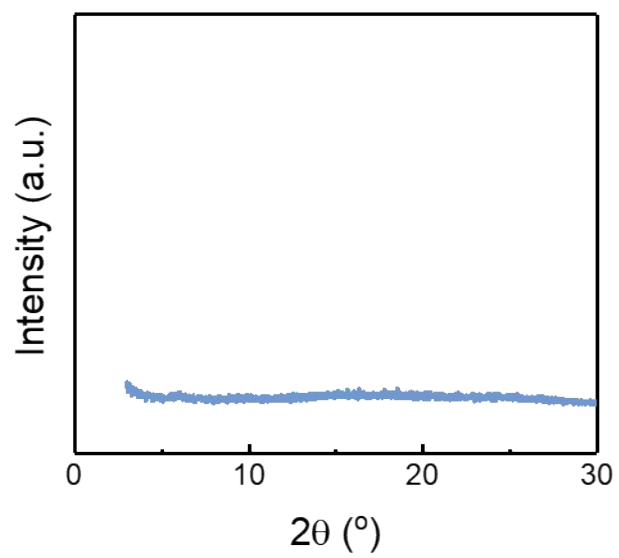


**Fig. S8** PXRD of **3** after magnetic measurement upon temperature increased to 400 K.

#### 4. X-ray crystallographic studies

Single-crystal X-ray diffraction data for complex **1**, **2** at 300K and **3** were collected using a Bruker SMART APEXII diffractometer coupled with a CCD area detector with graphite monochromated Mo K $\alpha$  ( $\lambda = 0.71073 \text{ \AA}$ ) radiation. Empirical absorption corrections were calculated using SADABS. Single-crystal X-ray diffraction data for complex **2** at 100 K were collected *via* an Oxford Cryo stream system on a XtaLAB PRO MM007-DW diffractometer system equipped with a RA-Micro7HF-MR-DW(Cu/Mo) X-ray generator and Pilatus3R-200K-A detector (Rigaku, Japan, Cu K $\alpha$ ,  $\lambda = 1.54178 \text{ \AA}$ ). The numerical absorption corrections were applied using the program of ABSCOR. The structures were solved using direct methods, which yielded the positions of all non-hydrogen atoms. These were refined first isotropically and then anisotropically. All the hydrogen atoms of the ligands were placed in calculated positions with fixed isotropic thermal parameters and included in the structure factor calculations in the final stage of full-matrix least-squares refinement. All calculations were performed using the SHELXTL system of computer programs.<sup>2,3</sup> Crystal data and structure refinement parameters are summarized in Tables S1. Containing the supplementary crystallographic data can be obtained free via [www.ccdc.cam.ac.uk/data\\_request/cif](http://www.ccdc.cam.ac.uk/data_request/cif)

**Table S1.** Crystal data and structure refinement for the square complexes.

□	1	2	2	3
Empirical formula	C <sub>70</sub> H <sub>64</sub> B <sub>2</sub> Co <sub>2</sub> F <sub>12</sub> Fe <sub>2</sub> N <sub>26</sub> P <sub>2</sub>	C <sub>81</sub> H <sub>84</sub> B <sub>2</sub> Co <sub>2</sub> F <sub>9</sub> F e <sub>2</sub> N <sub>26</sub> O <sub>5</sub> PS	C <sub>81</sub> H <sub>84</sub> B <sub>2</sub> Co <sub>2</sub> F <sub>9</sub> F e <sub>2</sub> N <sub>26</sub> O <sub>5</sub> PS	C <sub>115</sub> H <sub>166</sub> B <sub>2</sub> Co <sub>2</sub> F <sub>9</sub> F e <sub>2</sub> N <sub>26</sub> O <sub>10</sub> PS
Formula weight	1810.59	1986.95	1986.95	2557.94
<i>T</i> / K	100	100	300	100
Crystal system	monoclinic	triclinic	triclinic	monoclinic
Space group	<i>P</i> 2 <sub>1</sub> / <i>c</i>	<i>P</i> -1	<i>P</i> -1	<i>P</i> 2 <sub>1</sub> / <i>c</i>
<i>a</i> / Å	14.768(3)	12.3092(3)	12.5923(15)	17.1823(16)
<i>b</i> / Å	13.624(3)	14.2790(3)	14.4200(17)	17.7281(17)
<i>c</i> / Å	19.116(4)	14.8291(3)	15.0541(18)	21.953(2)
<i>α</i> / °	90	106.390(2)	104.622(2)	90
<i>β</i> / °	92.46(3)	96.544(2)	98.102(2)	94.260(2)
<i>γ</i> / °	90	105.982(2)	105.808(2)	90
<i>V</i> / Å <sup>3</sup>	3842.6(14)	2351.36(10)	2479.6(5)	6668.5(11)
<i>Z</i>	2	1	1	2
$\rho_{\text{calc}}$ / g cm <sup>3</sup>	1.565	1.403	1.331	1.274
$\mu$ / mm <sup>-1</sup>	0.927	6.157	0.729	0.560
F(000)	1840	1020	1020	2692.0
Reflections collected	19751	24996	12498	38196
Independent reflections	7533	8113	9052	15095
Goodness-of-fit on F <sup>2</sup>	1.028	1.279	1.036	1.056
Final <i>R</i> indexes [ <i>I</i> ≥ 2σ( <i>I</i> )]	R <sub>1</sub> = 0.0343, wR <sub>2</sub> = 0.0790	R <sub>1</sub> = 0.0931, wR <sub>2</sub> = 0.2924	R <sub>1</sub> = 0.0592, wR <sub>2</sub> = 0.1601	R <sub>1</sub> = 0.0859, wR <sub>2</sub> = 0.2448
Final <i>R</i> indexes [all data]	R <sub>1</sub> = 0.0475, wR <sub>2</sub> = 0.0851	R <sub>1</sub> = 0.1183, wR <sub>2</sub> = 0.3133	R <sub>1</sub> = 0.0874, wR <sub>2</sub> = 0.1802	R <sub>1</sub> = 0.1360, wR <sub>2</sub> = 0.2811
CCDC number	2189900	2189901	2189899	2189902

<sup>a</sup>  $R_1 = \frac{\sum (|F_o| - |F_c|)}{\sum |F_o|}$ ;  $wR_2 = \frac{\sum [w(F_o^2 - F_c^2)^2]}{\sum [w(F_o^2)^2]}^{1/2}$ ;  $w = 1/[\sigma_2(F_o^2) + (ap)^2 + bp]$ , where  $p = [\max(F_o^2, 0) + 2F_c^2]/3$ ; and  $Rw = \frac{\sum [w(|F_o| - |F_c|)^2/w|F_o|^2]}{\sum [w|F_o|^2]}^{1/2}$ , where  $w = 1/\sigma^2(|F_o|)$ .

**Table S2.** Selected bond distance (Å) and angle (°) for complex **1-3**.

□	<b>1</b>	<b>2</b>	<b>2</b>	<b>3</b>
<i>T</i> / K	100	100	300	100
Spin state	HS	LS	HS	LS
Co1-N1 / Å	2.1198(19)	1.948(5)	2.136(4)	1.930(4)
Co1-N2 / Å	2.168(2)	1.964(4)	2.113(4)	1.933(4)
Co1-N3 / Å	2.1366(19)	1.949(5)	2.126(4)	1.923(4)
Co1-N4 / Å	2.1308(19)	1.949(5)	2.124(3)	1.931(4)
Co1-N5 / Å	2.099(2)	1.910(5)	2.065(4)	1.884(4)
Co1-N6 / Å	2.121(2)	1.907(5)	2.079(3)	1.906(4)
Fe1-C1 / Å	1.925(3)	1.863(6)	1.930(5)	1.867(5)
Fe1-C2 / Å	1.923(2)	1.881(6)	1.881(6)	1.873(5)
Fe1-C3 / Å	1.933(2)	1.903(6)	1.920(4)	1.897(5)
Fe1-N8 / Å	1.9831(19)	2.039(5)	2.024(4)	2.038(4)
Fe1-N9 / Å	1.996(2)	2.059(5)	2.014(3)	2.057(4)
Fe1-N10 / Å	2.0226(19)	2.024(5)	1.995(3)	2.058(4)
Co-N (average) / Å	2.129	1.938	2.107	1.918
Fe-C/N (average) / Å	1.968	1.962	1.961	1.964
<sup>a</sup> Co-N-C / °	163.09(18)	171.3(5)	176.5(3)	177.3(3)
	160.36(18)	174.9(5)	173.2(3)	170.1(4)

<sup>a</sup>linkage between the Co sites and the Fe sites.

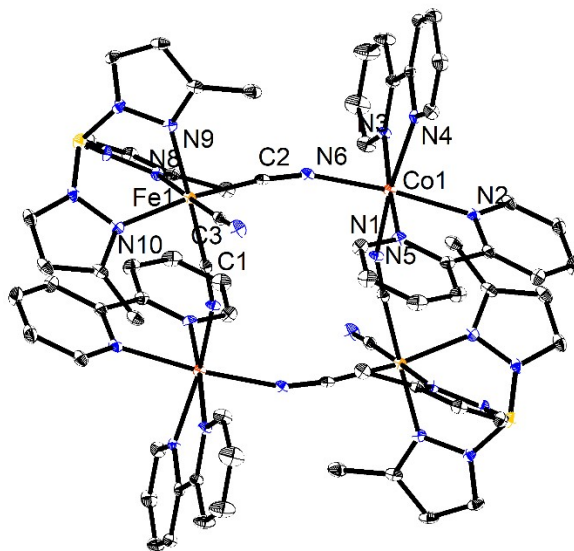


**Fig. S9** ORTEP diagram of the square molecule in **1** at 100 K with 50% thermal ellipsoid probability. Counteranions and hydrogen atoms are omitted for clarity.

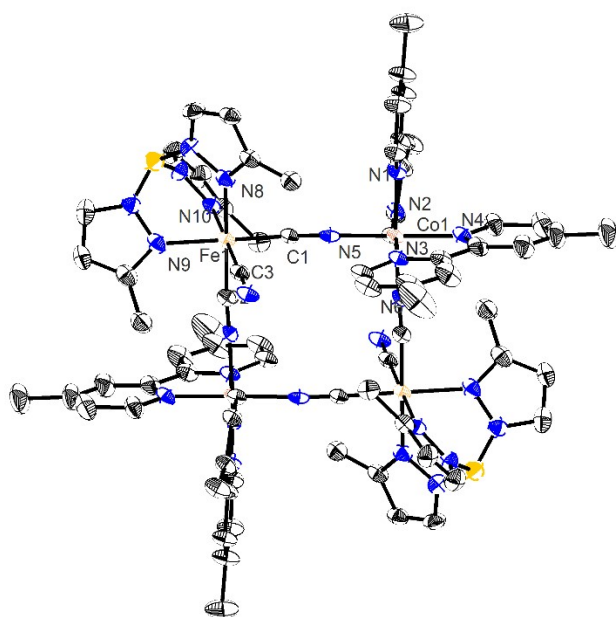


**Fig. S10** ORTEP diagram of the square molecule in **2** at 100 K with 50% thermal ellipsoid probability. Counteranions, solvent molecules, and hydrogen atoms are omitted for clarity.

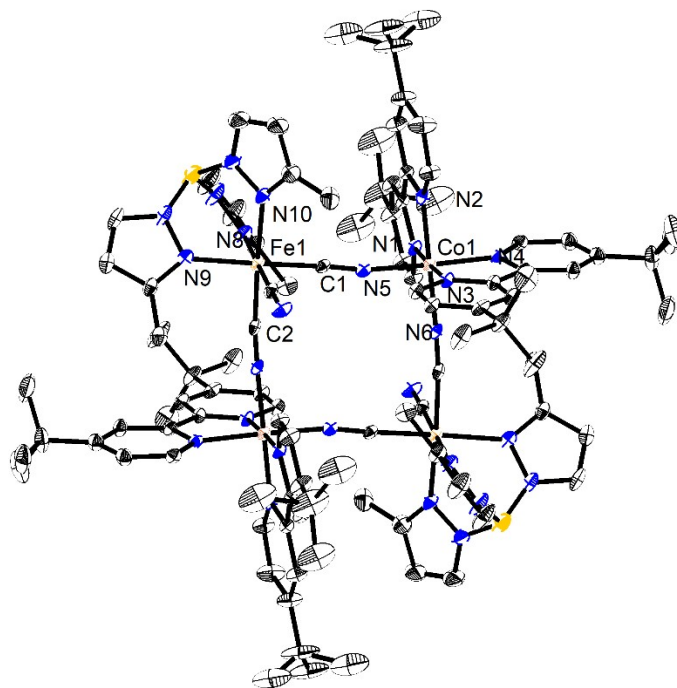


**Fig. S11** ORTEP diagram of the square molecule in **3** at 100 K with 50% thermal ellipsoid probability. Counteranions, solvent molecules, and hydrogen atoms are omitted for clarity.

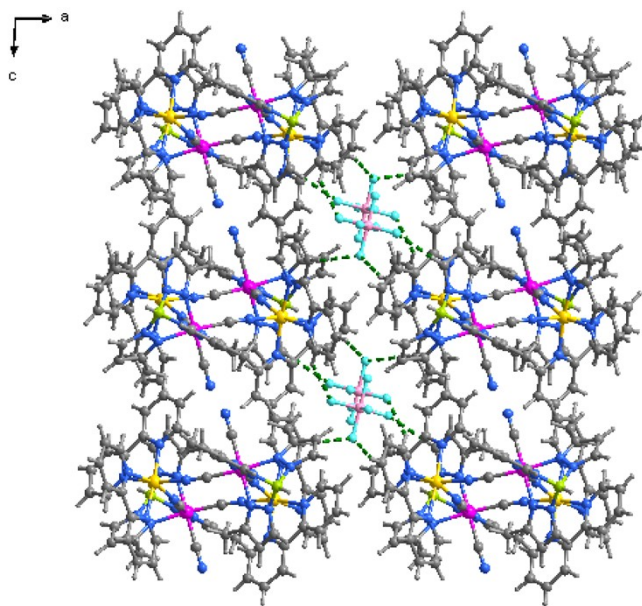


**Fig. S12** Crystal packing mode of **1** at 100 K.

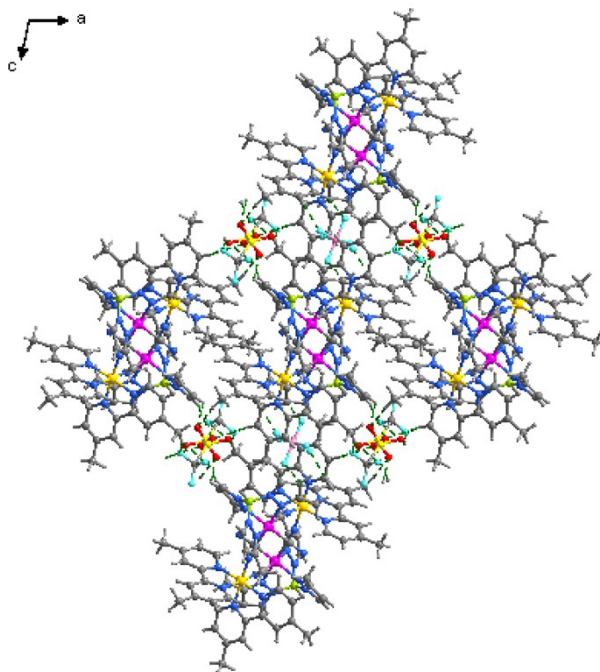


**Fig. S13** Crystal packing mode of **2** at 100 K.

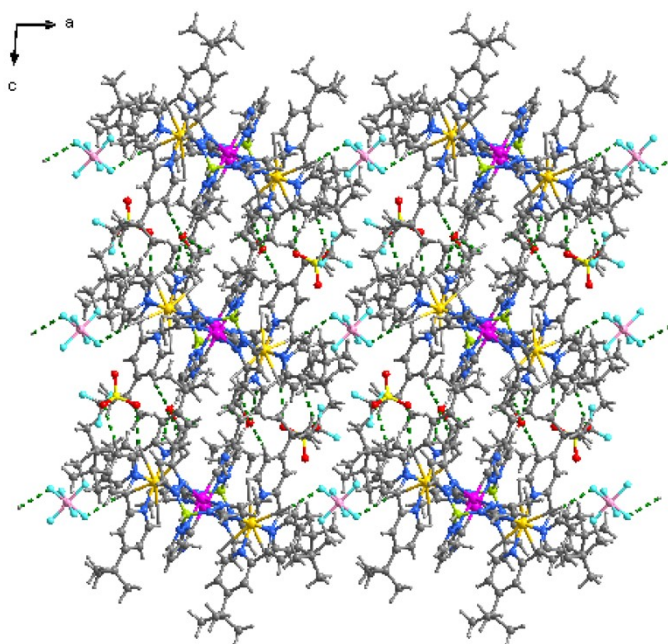


**Fig. S14** Crystal packing mode of **3** at 100 K.

## 5. Magnetic studies

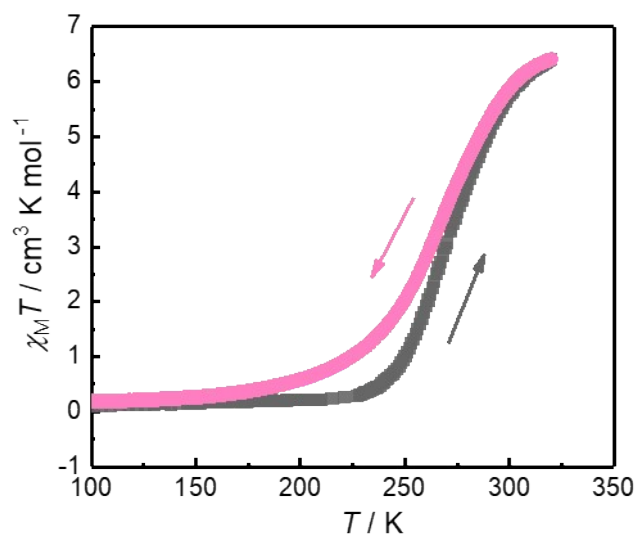


**Fig. S15**  $\chi_M T$  versus  $T$  plots of **2** in a heating-cooling cycle.

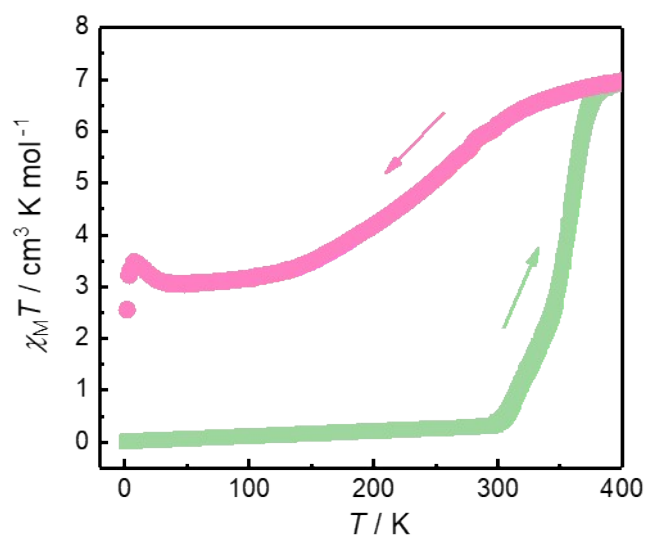


**Fig. S16**  $\chi_M T$  versus  $T$  plots of **3** in a heating-cooling cycle.

## 6. Thermogravimetric analyses (TGA)

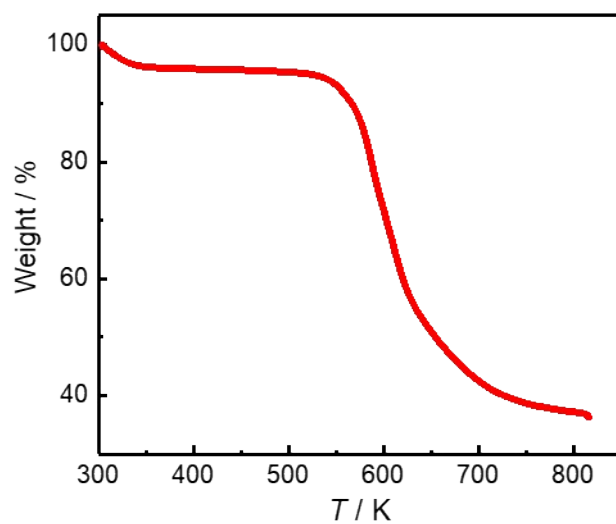


**Fig. S17** TG of 2.

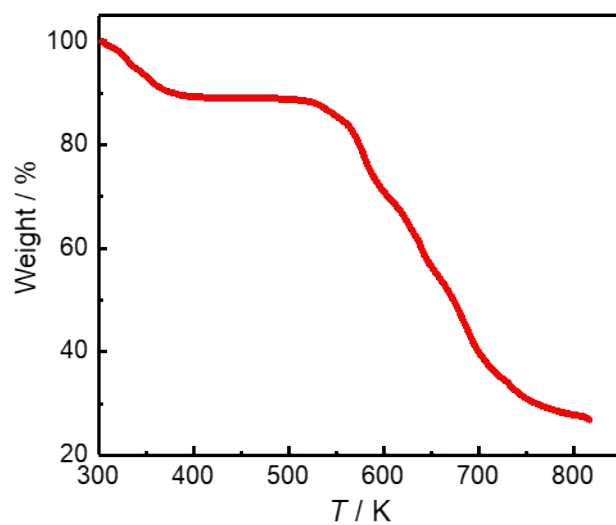


**Fig. S18** TG of 3.

## 7. Fourier-transform infrared (FT-IR) spectra

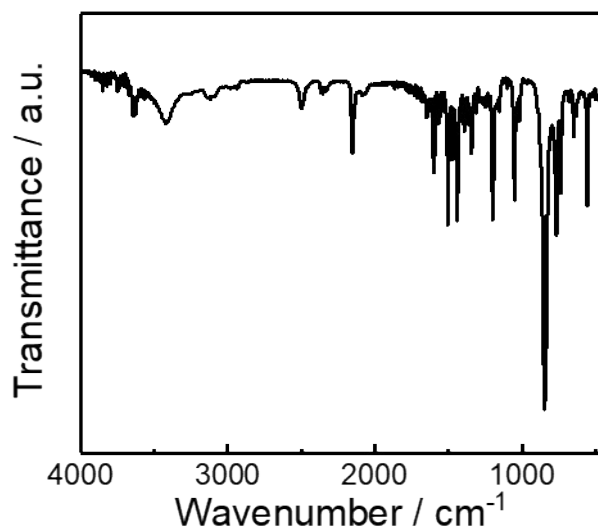


**Fig. S19** IR spectrum of **1** at room temperature.

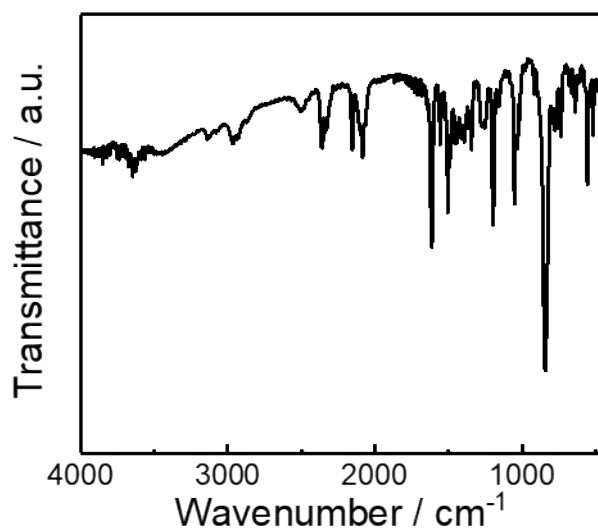


**Fig. S20** IR spectrum of **2** at room temperature.

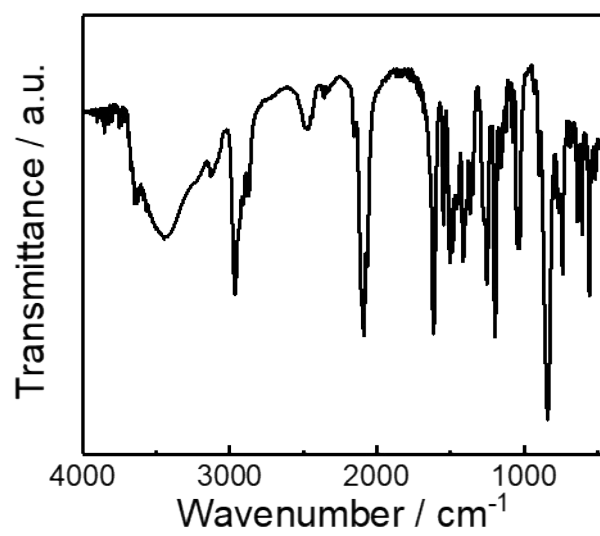


**Fig. S21** IR spectrum of **3** at room temperature.

## 8. $^{57}\text{Fe}$ Mössbauer spectra

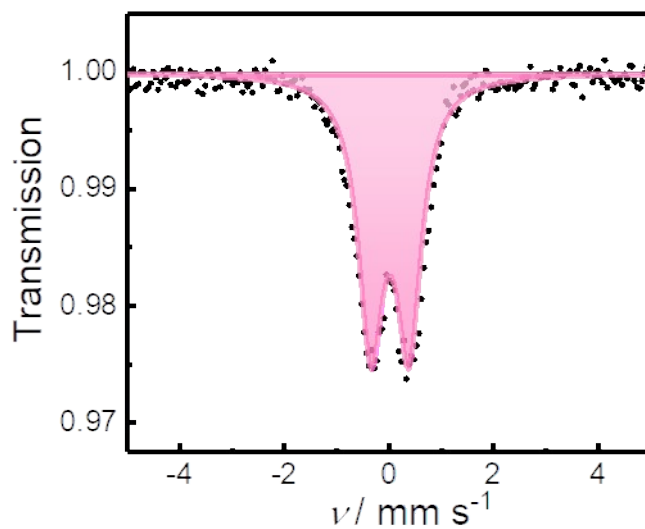


**Fig. S22**  $^{57}\text{Fe}$  Mössbauer spectrum of **1** at 300 K. The solid lines are Lorentzian curves calculated using the parameters in Supporting Information Table S3.

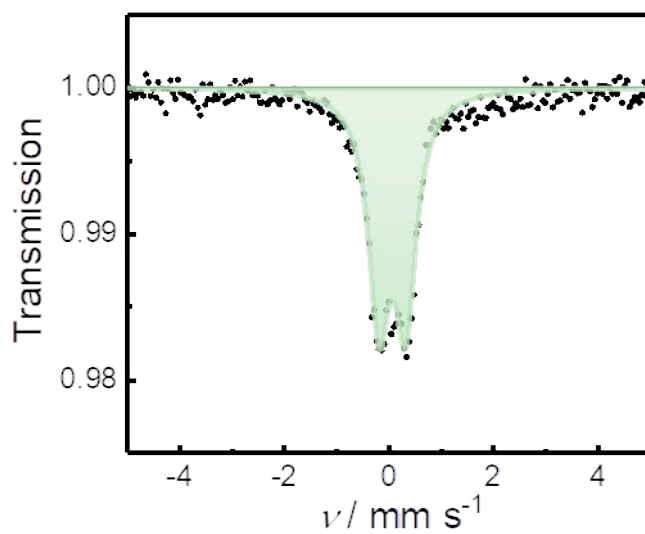


**Fig. S23**  $^{57}\text{Fe}$  Mössbauer spectrum of **3** at 300 K. The solid lines are Lorentzian curves calculated using the parameters in Supporting Information Table S3.

**Table S3.** Mössbauer parameters of complex **1-3**. 1re. Least-squares-fit parameters:  $\delta_{\text{IS}}$ ,  $\Delta E_{\text{Q}}$  and  $A$  are isomer shifts, quadrupole splitting, and area ratio, respectively. Parameters were calculated relative to  $\alpha$ -Fe foil.

		$\delta_{\text{IS}}$ (mm s <sup>-1</sup> )		$\Delta E_{\text{Q}}$ (mm s <sup>-1</sup> )		$A$ (%)	
		Fe <sup>II</sup> ls	Fe <sup>III</sup> ls	Fe <sup>II</sup> ls	Fe <sup>III</sup> ls	Fe <sup>II</sup> ls	Fe <sup>III</sup> ls
1	300 K		0.03		0.77		100
2	300 K	0.12	-0.07	0.49	0.68	19	81
	265 K	0.13	-0.06	0.46	0.75	61	39
	200 K	0.12		0.44		100	
3	300 K	0.06		0.51		100	

## 9. Various temperature UV-vis-Nir spectra in solution state

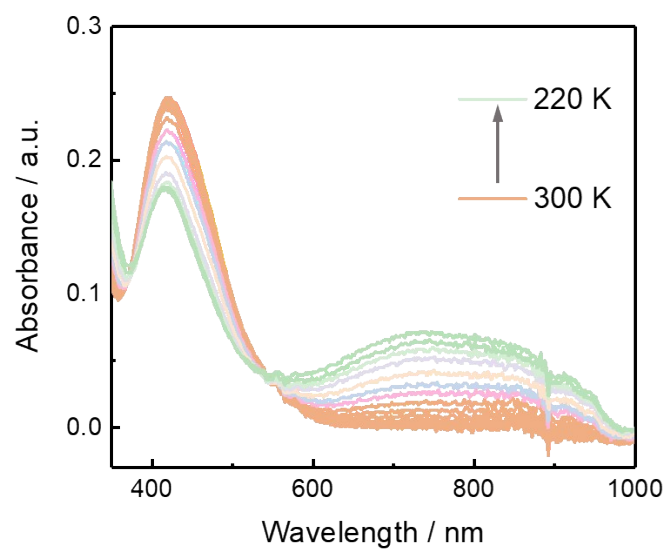


**Fig. S24** UV-vis-NIR spectral change of **1** in MeOH in the temperature range of 300-220 K.

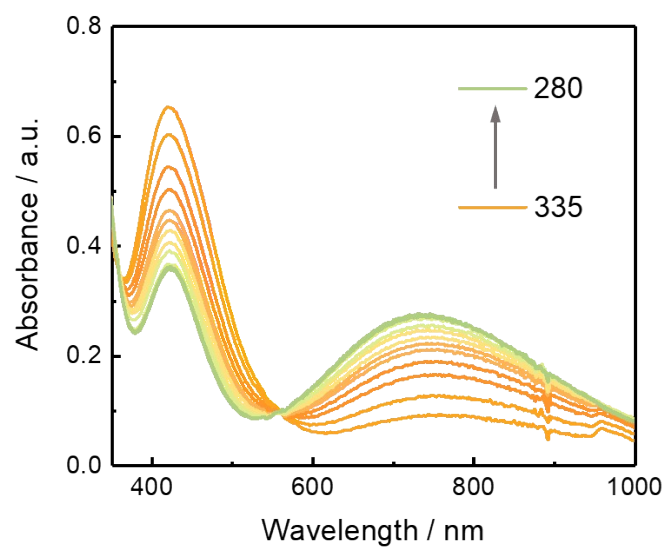


**Fig. S25** UV-vis-NIR spectral change of **3** in MeOH in the temperature range of 335-280 K.

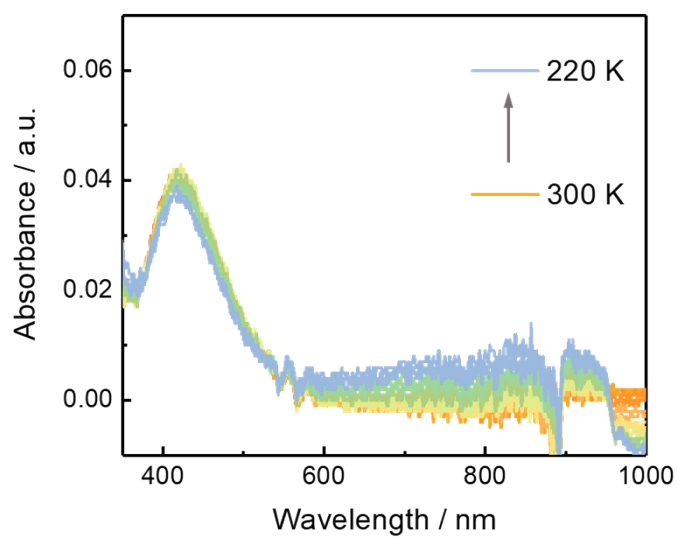


**Fig. S26** UV-vis-NIR spectral change of **1** in EtOH in the temperature range of 300-220 K.

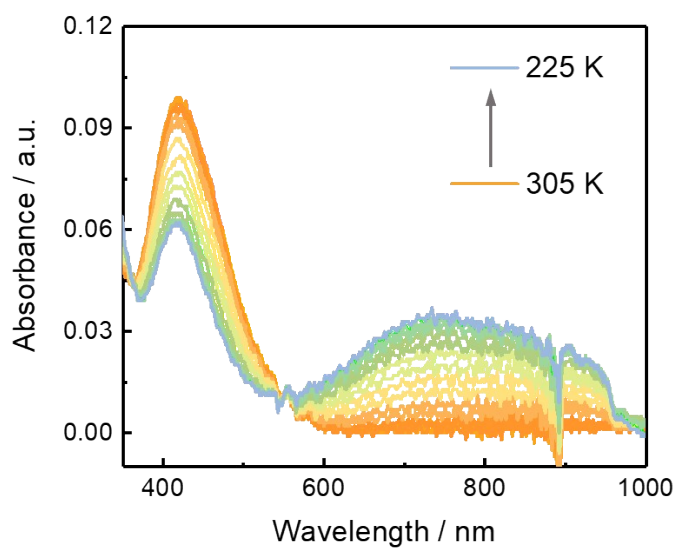


**Fig. S27** UV-vis-NIR spectral change of **2** in EtOH in the temperature range of 305-225 K.

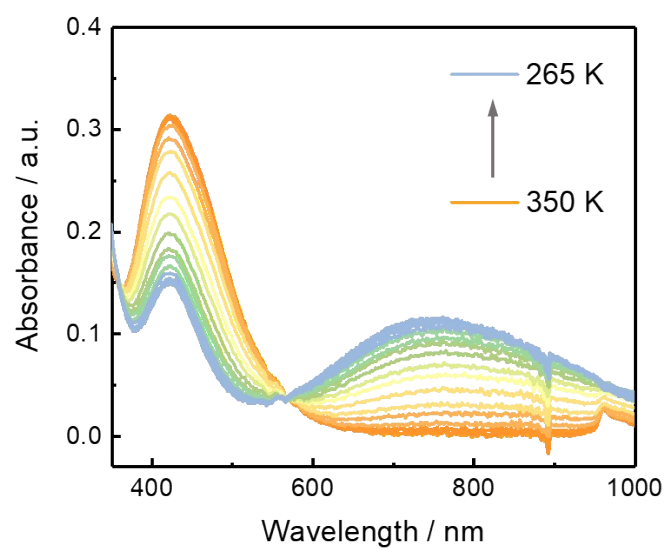


**Fig. S28** UV-vis-NIR spectral change of **3** in EtOH in the temperature range of 350-265 K.

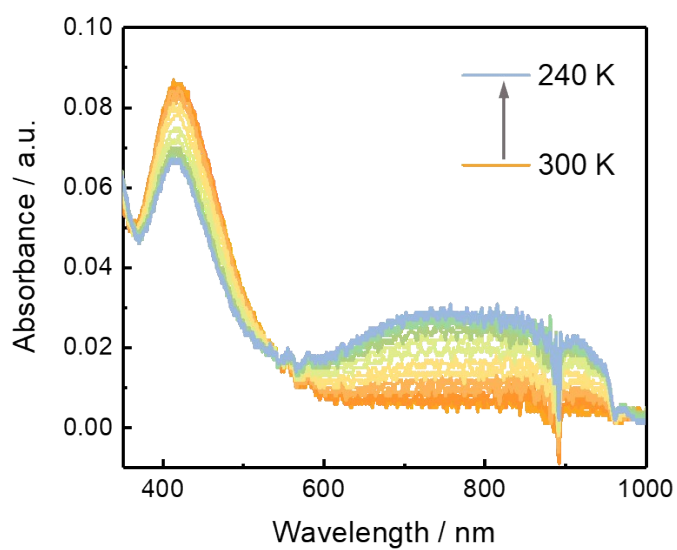


**Fig. S29** UV-vis-NIR spectral change of **2** in *n*-PrOH in the temperature range of 300-240 K.

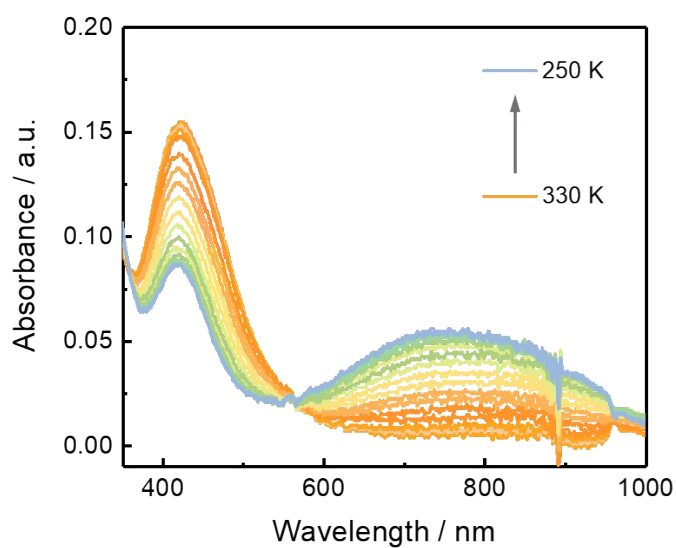


**Fig S30** UV-vis-NIR spectral change of **3** in *n*-PrOH in the temperature range of 330-250 K.

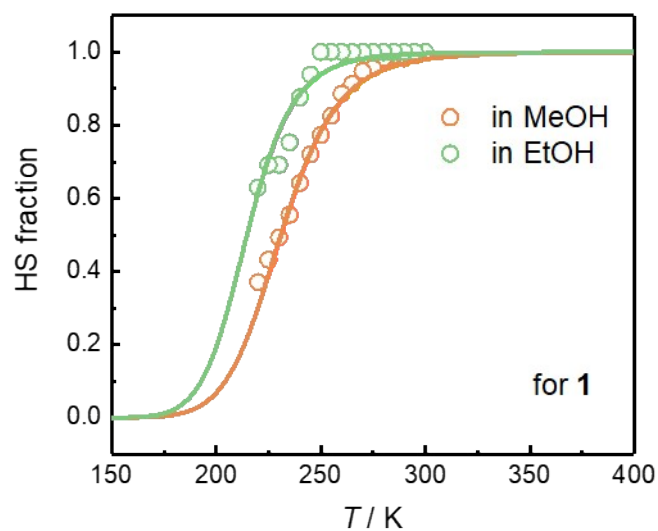


**Fig. S31**  $[(\text{Co}^{\text{II}}_{\text{HS}})_2(\text{Fe}^{\text{III}}_{\text{LS}})_2]$  fractions versus temperature plots of **1** in various solvents.

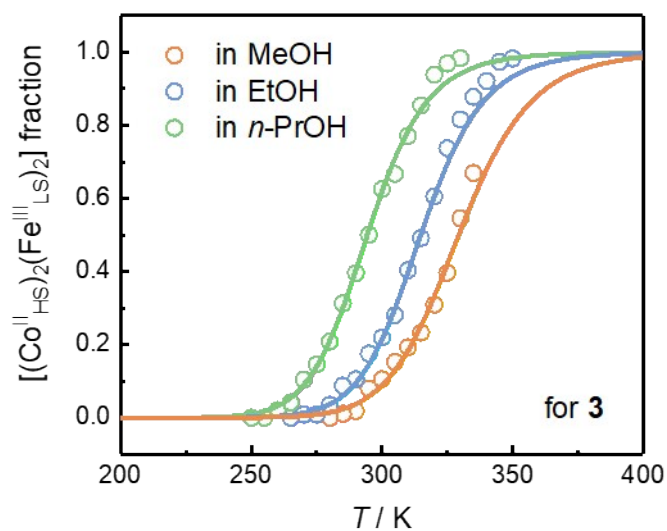


**Fig. S32**  $[(\text{Co}^{\text{II}}_{\text{HS}})_2(\text{Fe}^{\text{III}}_{\text{LS}})_2]$  fractions versus temperature plots of **3** in various solvents.

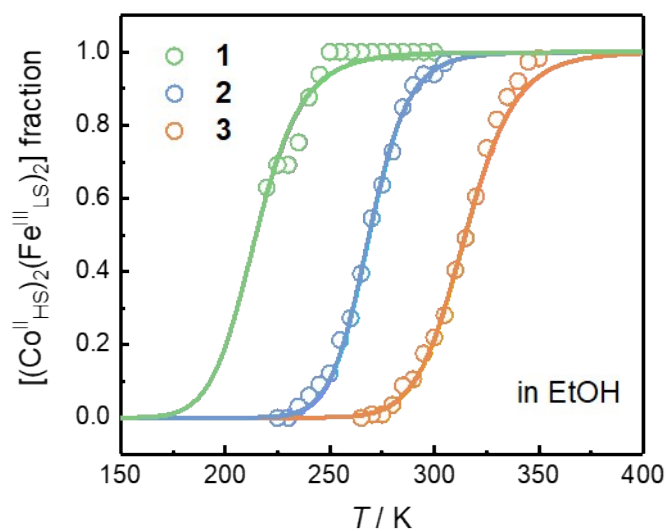


**Fig. S33**  $[(\text{Co}^{\text{II}}_{\text{HS}})_2(\text{Fe}^{\text{III}}_{\text{LS}})_2]$  fractions versus temperature plots of **1-3** in EtOH.

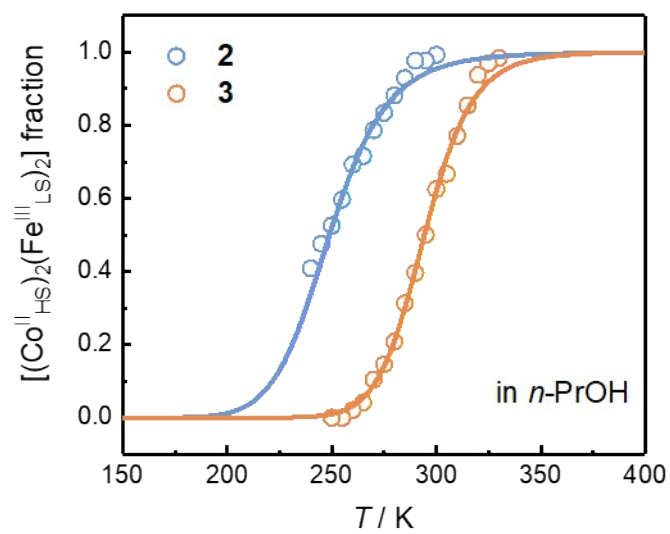


**Fig. S34**  $[(\text{Co}^{\text{II}}_{\text{HS}})_2(\text{Fe}^{\text{III}}_{\text{LS}})_2]$  fractions versus temperature plots of **2** and **3** in *n*-PrOH.

## 10. Electrochemical studies

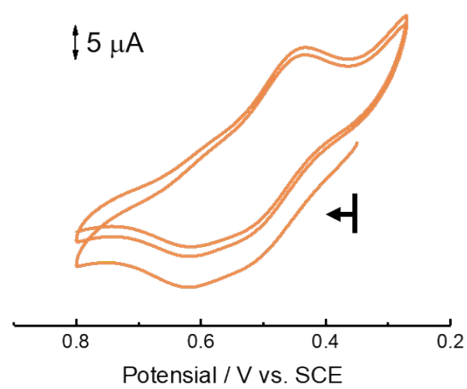


**Fig. S35** Cyclic voltammogram of complex **1** in the range of +0.27 to +0.80 V.

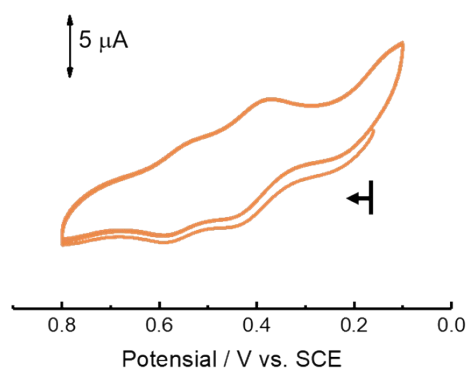


**Fig. S36** Cyclic voltammogram of complex **2** in the range of +0.1 to +0.80 V.

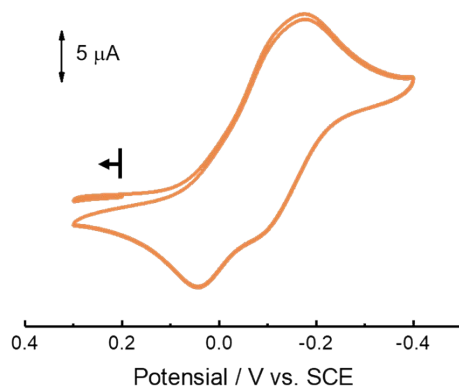


**Fig. S37** Cyclic voltammogram of complex **3** in the range of +0.3 to -0.40 V.

**Table S4.** CV Data (vs. SCE at room temperature) for the Co<sup>II</sup>/Co<sup>III</sup> redox waves in **1**, **2** and **3**.

Complex	Resting potential (V)	Oxidation state	$E_{pa}$ (V)	$E_{pc}$ (V)	$E_{1/2}$ (V) <sup>a</sup>
<b>1</b>	0.35	$[(Co^{II})_2(Fe^{III})_2]^{2+}/[(Co^{II})(Co^{III})(Fe^{III})_2]^{3+}$	0.440	0.518	0.479
		$[(Co^{II})(Co^{III})(Fe^{III})_2]^{3+}/[(Co^{III})_2(Fe^{III})_2]^{4+}$	0.622	0.594	0.608
<b>2</b>	0.16	$[(Co^{II})_2(Fe^{III})_2]^{2+}/[(Co^{II})(Co^{III})(Fe^{III})_2]^{3+}$	0.435	0.372	0.403
		$[(Co^{II})(Co^{III})(Fe^{III})_2]^{3+}/[(Co^{III})_2(Fe^{III})_2]^{4+}$	0.599	0.540	0.57
<b>3</b>	0.2	$[(Co^{II})(Co^{III})(Fe^{II})_2]^+ / [(Co^{III})_2(Fe^{II})_2]^{2+}$	-	-	-
		$[(Co^{II})_2(Fe^{II})_2] / [(Co^{II})(Co^{III})(Fe^{II})_2]^+$	0.083	0.175	-0.129
			0.044	0.106	0.075

<sup>a</sup>  $E_{1/2} = (E_{pa} + E_{pc})/2$

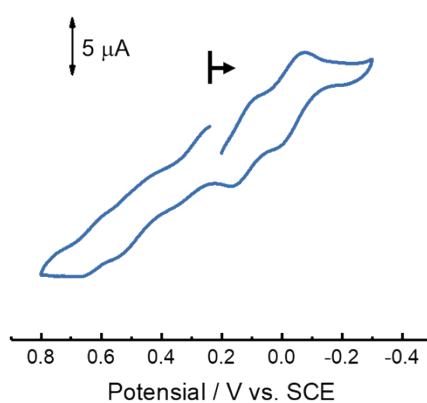


**Fig. S38** Cyclic voltammogram of complex **1** in the range of +0.8 to -0.3 V.

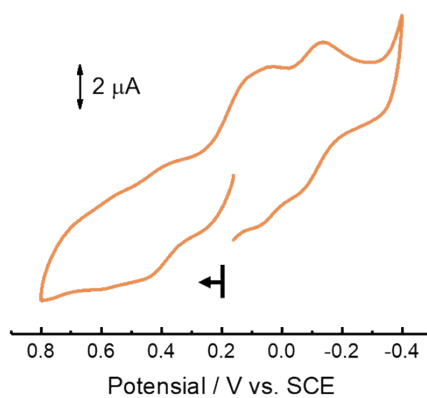


**Fig. S39** Cyclic voltammogram of complex **2** in the range of +0.8 to -0.4 V.

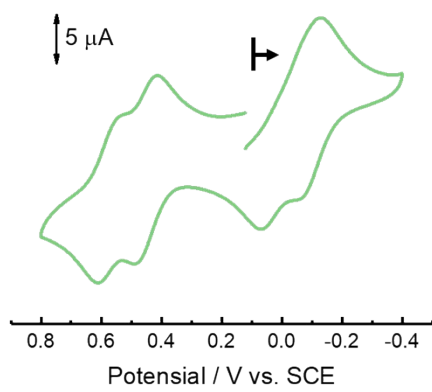


**Fig. S40** Cyclic voltammogram of complex **3** in the range of +0.8 to -0.4 V.

## 11. Theoretical calculation

All calculations were performed with Gaussian09 package<sup>[2]</sup> under B3LYP-D3<sup>[3]</sup>/6-31+G(d, p)<sup>[4]</sup> theoretical level. The geometries of  $[\text{CoL}]^{3+}$  cations were firstly optimized, and their reduced forms,  $[\text{CoL}]^{2+}$ , by adding an extra electron manually. The redox potential of the reduction process was calculated by the following formula:

$$E_{redox} = (G_{3+} - G_{2+})/F$$

Where  $G_{3+}$  and  $G_{2+}$  are the Gibbs free energy of the  $[\text{CoL}]^{3+}$  and  $[\text{CoL}]^{2+}$  cations, respectively,  $F$  is the Faraday constant.

The results were shown in Fig. S41.

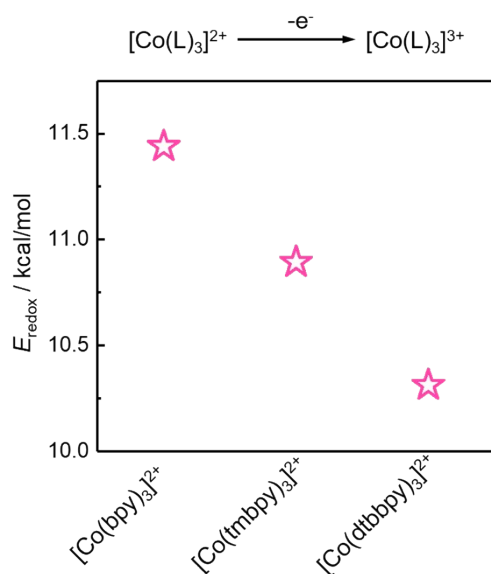


**Fig. S41** Redox potential for the oxidation process from  $[\text{Co}(\text{L})_3]^{2+}$  to  $[\text{Co}(\text{L})_3]^{3+}$ .

## 12. References

1. Li, D.; Parkin, S.; Wang, G.; Yee, G. T.; Holmes, S. M. *Inorg. Chem.* **2006**, *45*, 1951-1959.
2. Hübschle, C. B.; Sheldrick, G. M.; Dittrich, B. *J. Appl. Crystallogr.* **2011**, *44*, 1281-1284.
3. Sheldrick, G. M. *Acta Crystallogr. A* **2008**, *64*, 112-122.
4. Frisch, G. W. T. M. J.; Schlegel, H. B.; Scuseria, G. E.; Robb, M. A.; Cheeseman, J. R.; Scalmani, G.; Barone, V.; Mennucci, B.; Petersson, G. A.; Nakatsuji, H.; Caricato, M.; Li, X.; Hratchian, H. P.; Izmaylov, A. F.; Bloino, J.; Zheng, G.; Sonnenberg, J. L.; Hada, M.; Ehara, M.; Toyota, K.; Fukuda, R.; Hasegawa, J.; Ishida, M.; Nakajima, T.; Honda, Y.; Kitao, O.; Nakai, H.; Vreven, T.; Montgomery, Jr. J. A.; Peralta, J. E.; Ogliaro, F.; Bearpark, M.; Heyd, J. J.; Brothers, E.; Kudin, K. N.; Staroverov, V. N.; Kobayashi, R.; Normand, J.; Raghavachari, K.; Rendell, A.; Burant, J. C.; Iyengar, S. S.; Tomasi, J.; Cossi, M.; Rega, N.; Millam, J. M.; Klene, M.; Knox, J. E.; Cross, J. B.; Bakken, V.; Adamo, C.; Jaramillo, J.; Gomperts, R.; Stratmann, R. E.; Yazyev, O.; Austin, A. J.; Cammi, R.; Pomelli, C.; Ochterski, J. W.; Martin, R. L.; Morokuma, K.; Zakrzewski, V. G.; Voth, G. A.; Salvador, P.; Dannenberg, J. J.; Dapprich, S.; Daniels, A. D.; Farkas, Ö.; Foresman, J. B.; Ortiz, J. V.; Cioslowski, J.; Fox, D. J. Gaussian, Inc., Wallingford CT, *Gaussian 09, Inc. Wallingford CT*, **2009**.
4. a) A. D. Becke, *J. Chem. Phys.* **1993**, *98*, 5648-5652; b) S. Grimme, J. Antony, S. Ehrlich, H. Krieg, *J. Chem. Phys.* **2010**, *132*, 154104.
5. P. C. Hariharan, J. A. Pople, *Theor. Chim. Acta* **1973**, *28*, 213-222.